

Conformation Analysis of Ferrocene and Decamethylferrocene via Full-Potential Modeling of XANES and XAFS Spectra

J. D. Bourke,[†] M. T. Islam,[‡] S. P. Best,[§] C. Q. Tran,^{||} F. Wang,[⊥] and C. T. Chantler^{*,†}

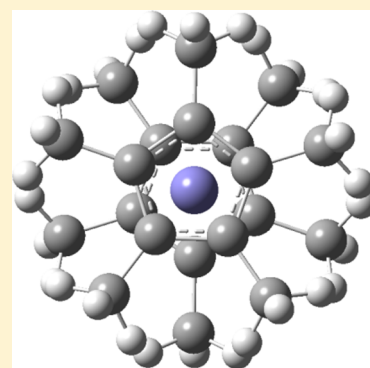
[†]School of Physics, [‡]Schools of Physics and Chemistry, and [§]School of Chemistry, University of Melbourne, Parkville, Victoria 3010 Australia

^{||}School of Physics, La Trobe University, Melbourne, Victoria 3086, Australia

[⊥]Department of Chemistry and Biotechnology, Swinburne University of Technology, Hawthorn, Victoria 3122, Australia

S Supporting Information

ABSTRACT: Recent high-accuracy X-ray absorption measurements of the sandwich organometallics ferrocene (Fc) and decamethylferrocene (DmFc) at temperatures close to liquid helium are compared with new full-potential modeling of X-ray absorption fine structure (XAFS) covering the near-edge region (XANES) and above up to $k = 7 \text{ \AA}^{-1}$. The implementation of optimized calculations of the oscillatory part of the spectrum from the package FDMX allows detailed study of the spectra in regions of the photoelectron momentum most sensitive to differences in the molecular stereochemistry. For Fc and DmFc, this corresponds to the relative rotation of the cyclopentadienyl rings. When applied to high-accuracy XAFS of Fc and DmFc, the FDMX theory gives clear evidence for the eclipsed conformation for Fc and the staggered conformation for DmFc for frozen solutions at ca. 15 K. This represents the first clear experimental assignment of the solution structures of Fc and DmFc and reveals the potential of high-accuracy XAFS for structural analysis.



The physical and electronic structures of ferrocene (Fc), decamethylferrocene (DmFc), and analogous organometallic sandwich structures have been the subject of a great many recent studies^{1,2} stimulated by their applications in catalysis,³ fuel additives, anticancer treatments,⁴ and pharmaceuticals.⁵ Their characteristic co-ordination geometry also provide a unique test case for structural analysis using X-ray absorption fine structure (XAFS) spectroscopy, the high-frequency oscillatory component of the photoelectric X-ray absorption spectrum immediately following an ionization edge. The XAFS provides detailed signatures of the local atomic (i.e., molecular) structure around the absorbing atom.

This work follows a recent experimental, theoretical, and analytical investigation of Fc and DmFc centered on the high absolute-accuracy measurement Hybrid Technique for XAFS.⁶ This Hybrid Technique was used to measure XAFS for dilute Fc and DmFc compounds as frozen solutions at ca. 15 K. These spectra were then compared with the current most popular *ab initio* theoretical calculations based on a variety of structural models,⁷ and the results were used to infer the conformation of Fc and DmFc in their lowest energy forms.

Here, we investigate the implementation of new full-potential modeling of photoelectron scattering to quantify the XAFS accurately in the near-edge region; that is, for energies $\leq 60 \text{ eV}$ above the ionization edge or photoelectron momenta $< 4 \text{ \AA}^{-1}$, referred to as X-ray absorption near-edge structure (XANES). The models used in previous work are highly sophisticated and in widespread use; however, they do not describe the detailed form of the electronic potential between atomic cores, and are

thus unable to model the XANES region to discern subtle features sensitive to the conformation of the molecule.⁸

Experimental work on Fc and DmFc over several decades has pointed to their structures consisting of an iron atom “sandwiched” between two parallel pentagonal rings of $(\text{CH})_5$ (for Fc) or $(\text{C}(\text{CH}_3))_5$ (for DmFc) in a staggered geometry corresponding to a 36° rotational offset between the rings. Density functional theory (DFT), however, often predicts that an eclipsed geometry for Fc, with no rotational offset, will produce a lower energy and should thus be more stable. This suggestion has recently been supported by theory,⁷ and is consistent with the high-energy XAFS analysis in the precursor to this work.⁶ A schematic of the basic conformational states for both Fc and DmFc is provided in Figure 1.

Despite the promise of these early investigations, it is at low photoelectron energy, in the XANES region, that the greatest sensitivity to conformation properties can be obtained, and thus the most rigorous conclusions about the ground-state structure of these molecules. In particular, the long-range scattering paths that simultaneously probe both of the rings find their strongest relative contribution and hence discriminatory signature in the XANES and extended XANES region.

The theoretical basis for this work is the FDMX approach developed by Bourke, Chantler, and Joly,⁹ built on the full-potential modeling platform of FDMNES.¹⁰ FDMX calculates

Received: June 22, 2016

Accepted: July 8, 2016

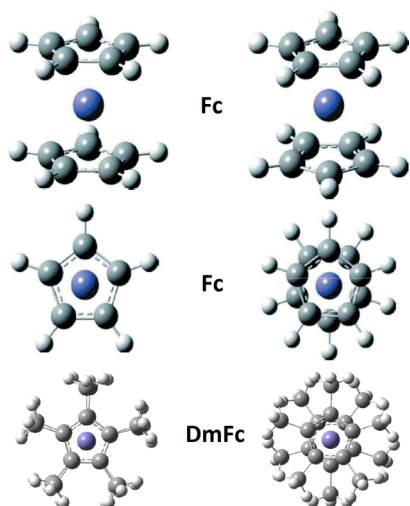


Figure 1. Schematic of conformers for Fc and DmFc, showing eclipsed (left) and staggered (right) geometries corresponding to D_{5h} and D_{5d} symmetries, respectively.

photoelectric absorption spectra by mapping the final state wave function of the photoelectron within a spherical cluster in the vicinity of the excited atom. This mapping takes place over a finite grid, allowing an approximation to the Schrödinger Equation to determine the coulomb potential and electronic wave function in a self-consistent manner and with accuracy determined primarily by the grid density. This final state photoelectron wave function, modulated by scattering from neighboring atoms, is then transformed with the ground-state core electron wave function via Fermi's golden rule to compute the total absorption cross section at each energy. The energy-dependent interference of the emitted and returning photoelectron wave functions leads to the oscillatory nature of the XAFS spectrum.

Theoretical spectra evaluated using FDMX and based on structures detailed in the previous investigation⁶ were tested with our high-accuracy measurements of XANES and XAFS of Fc and DmFc. Calculations were refined using a fitting algorithm that is able to adjust spectral parameters such as background absorption (unmodulated absorption from atomic Fe) and the theoretical near-edge offset,¹¹ as well as physical parameters including thermal disorder,¹² the Fermi level, chemical shift, and the core-hole lifetime (from tabulations). This procedure enables the oscillatory components of the spectra to be isolated and compared directly with the experimental data, and for the best fits to be determined using each potential structural geometry. Goodness of fit for each structure is quantified robustly using χ_r^2 , the mean-square deviation from experiment weighted by the absolute-scale uncertainties of the data.

Three prototype staggered structures, and their eclipsed analogues, were considered as models of the structure of Ferrocene. These are based on the previous XAFS investigation using multiple-scattering theory.⁶ The structures include one based on a regularisation and refinement of bond lengths reported by Seiler and Dunitz,¹³ which we refer to here as an *aggregated crystal structure*, and two *ab initio* structures—one using CCSD(T) and a DFT-generated B3LYP type optimization.⁷ In Figure 2 we show the XAFS structures calculated using the full-potential FDMX theory based on the eclipsed and

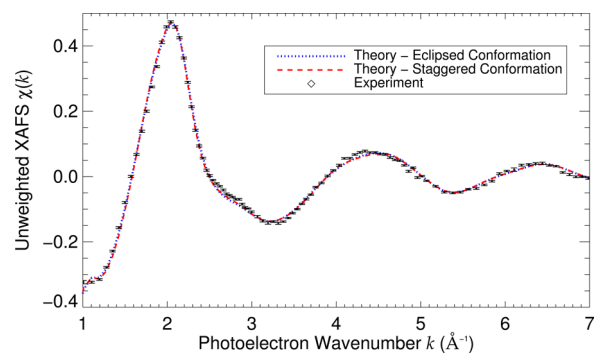


Figure 2. Unweighted XAFS spectra of Ferrocene using eclipsed and staggered conformations based on the aggregated crystal structure of Seiler and Dunitz (Table 6 in ref 6). Comparison with the experimental data demonstrates good qualitative agreement but quite subtle conformational dependence, suggesting extremely high quality theory, and experiments are needed to extract the necessary structural information.

staggered versions of the aggregated crystal structure, compared with the experimental result.

Important features of this comparison are the excellent qualitative agreement between theory and experiment across the entire energy range considered, and the quite subtle difference between the eclipsed and staggered conformations. Indeed, the same features are present with the CCSD(T) and B3LYP DFT structures, and persist in the analysis of DmFc. Detailed plots of k^2 -weighted spectra are available as [Supporting Information](#) online. It is clear from the current comparison, however, that the small differences between spectra mean that visual comparisons between the competing structures provide no insight.

Given the extremely small differences between the conformers, they can only be meaningfully probed with extremely accurate experimental data of the kind we have collected. Standard measurements, which typically report higher uncertainties than the Hybrid Technique by an order of magnitude or more,¹⁴ would inevitably conclude that the eclipsed and staggered geometries were indistinguishable. Past advanced experiment, theory and analysis, but especially theory, has concluded that there are no differences between the XAFS predictions of the two conformers, so that XAFS can not distinguish between the moieties.^{15,16} Conversely, we find that the differences calculated or experimental, while subtle, can be observable with careful measurement and analysis.

Analysis is aided by optimizing physical and computational parameters in an energy-dependent fashion. This is partly required by the complex nature of the background absorption,¹⁷ but is also necessary due to the significant energy-dependence of the thermal disorder,¹² and the natural energy-dependent weighting of structural contributions in XANES and XAFS spectra.

In order to assess appropriate limits for different energy regimes, we illustrate in Figure 3 the differences between the equivalent staggered and eclipsed spectra for each prototype structure. Although there are some differences in the impact of conformational change between each prototype structure, the most significant changes in the XAFS due to angle of rotation of the $(\text{CH})_5$ rings consistently occur in the XANES region, at photoelectron momenta below $k = 3 \text{ \AA}^{-1}$. We therefore assess each potential structure of Fc in terms of a fit to experiment

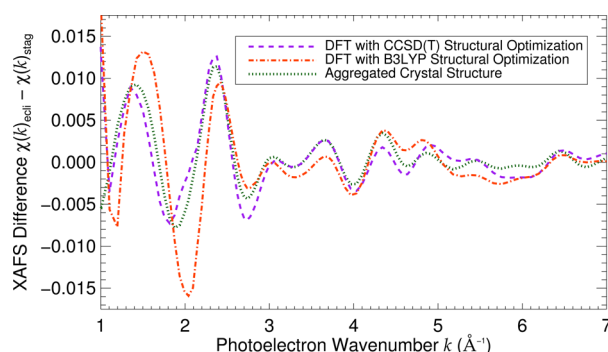


Figure 3. Differences between the oscillatory part of the spectrum $\chi(k)$ of the eclipsed and staggered conformations of Ferrocene, based on the three different refined prototype structures - Seiler and Dunitz (refined,⁶ Table 6), CCSD(T) theory (ibid, Table 7), and B3LYP DFT (ibid, Table 7). This demonstrates the significantly greater sensitivity of the extended XANES region to differences in conformational geometry.

over three photoelectron momentum ranges: $k = 1.0\text{--}3.0 \text{ \AA}^{-1}$, $k = 1.0\text{--}7.0 \text{ \AA}^{-1}$, and $k = 3.0\text{--}7.0 \text{ \AA}^{-1}$.

The first structure we consider is the CCSD(T) optimization of Fc, designed to generate the lowest energy-state structures for isolated Fc at 0 K with either eclipsed or staggered geometry. The resulting χ_r^2 values for this and other structures are given in Table 1. Perhaps counterintuitively given the prior

Table 1. Goodness of Fit for Eclipsed and Staggered Conformers Based on Prototype Geometries over Different k Ranges^a

Ferrocene			
k range (\AA^{-1})	1.0–3.0	1.0–7.0	3.0–7.0
CCSD(T) eclipsed χ_r^2	14.4	14.3	7.43
CCSD(T) staggered χ_r^2	19.6	14.0	7.01
B3LYP eclipsed χ_r^2	20.1	24.4	5.12
B3LYP staggered χ_r^2	35.2	35.2	5.14
ACS eclipsed χ_r^2	12.8	14.0	8.02
ACS Staggered χ_r^2	17.0	15.6	8.01
Decamethylferrocene			
k range (\AA^{-1})	1.5–3.5	1.5–7.0	3.5–7.0
Islam et al. eclipsed χ_r^2	9.02	11.4	6.37
Islam et al. staggered χ_r^2	8.16	10.4	5.76
Makal et al. eclipsed χ_r^2	7.69	6.71	3.49
Makal et al. staggered χ_r^2	6.91	5.32	2.97

^aHere ACS refers to the aggregated crystal structure, reported in Islam et al.⁶ and derived as a refinement of the structure given by Seiler et al.¹³

literature, the fit is marginally better in the higher-energy region ($\sim 6\%$) when a *staggered* geometry is used, but the eclipsed geometry remains significantly better at lower energies ($\sim 27\%$). We expect greater sensitivity at lower photoelectron energies and low k , but it may seem odd to find different conclusions in the two different energy regimes. We must therefore make the important note that different k -ranges probe different contributions to the structure. Higher energy oscillations are dominated by single-scattering events where, for example, the Fe–C bond length is probed directly, while in the XANES region multiple-scattering events are much stronger, allowing us to probe distances involving both carbon rings, and hence the conformation of the molecule, for the first time. These current

results for the CCSD(T) prediction therefore strongly favor an eclipsed conformer.

When using the B3LYP optimization of DFT, in the sensitive region below $k = 3.0 \text{ \AA}^{-1}$ the eclipsed structure performs dramatically (43%) better than the staggered. This result is consistent with Figure 3, which suggested that the B3LYP optimization would show the greatest difference between conformers at low photoelectron energy.

Finally, the *aggregated crystal structure* given as ACS in Table 1 was an optimized structure that provided the best model fit of XAFS in the earlier investigation using FEFF theory for $k = 3\text{--}12 \text{ \AA}^{-1}$, and in the sensitive region here also provides the best fit and strongest evidence for the stability of the eclipsed conformation. Again, the range $k = 3.0\text{--}7.0 \text{ \AA}^{-1}$ does not differentiate between the conformations, but significant differences are seen below 3.0 \AA^{-1} , with the eclipsed geometry performing 25% better. This consistency in the low-energy regime, where the nature of XANES spectra is expected to amplify the effects of conformational variation, is a strong indicator that the Fc molecules observed by the experiment are indeed in the eclipsed geometry. It is also instructive that for Fc, parts of the spectrum (high- k) typically probed by alternative theoretical techniques (FEFF and other approaches) are not as sensitive a probe of the molecular stereochemistry.

For this new theoretical approach to be considered accurate and robust, however, it must be equally able to predict correct stereochemistry where there currently is strong consensus. DmFc is well-considered to be in a staggered conformation due to steric hindrance of the methyl groups (Figure 1), with no suggestion of a stable eclipsed conformer in solution. We therefore use it as a benchmark for our analysis.

For DmFc we use two prototype structures (staggered) reported in the literature, and their analogues rotated into an eclipsed geometry. Unlike the case of Fc, we omit the hydrogenic contributions for DmFc due to the prohibitive size of the molecule and the large disorder of the hydrogen positions. The first prototype structure used is from the preceding work, Islam et al.,⁶ and is derived loosely from a regularized version of a structure reported by Freyberg et al.¹⁸ The second is from the low temperature experimental charge density analysis of Makal et al.,¹⁹ which appears to be a more authoritative structural determination. This structure was reported as a staggered geometry with four planar carbon ligands and a nonplanar carbon completing the pentagonal structure of the first co-ordination shell. The eclipsed analogue was constructed using a mirror symmetry parallel to the four-atom carbon plane and intersecting with the absorbing Fe atom. We once again assess the energy regions of interest by plotting the differences between the XAFS spectra calculated using eclipsed and staggered geometries (Figure 4).

We have adjusted the lower limit to our energy range for DmFc, as compared with Fc, due to the chemical shift in the edge position (vacuum level). Guided by Figure 4, we assessed the DmFc data in energy windows covering the ranges $k = 1.5\text{--}3.5 \text{ \AA}^{-1}$, $k = 1.5\text{--}7.0 \text{ \AA}^{-1}$, and $k = 3.5\text{--}7.0 \text{ \AA}^{-1}$.

The χ_r^2 values for the prototype DmFc structures are given in Table 1. Consistent with the larger amplitude of the $\chi_{\text{eclipsed}}(k) - \chi_{\text{staggered}}(k)$ function for the more complex DmFc molecule, significant distinctions between the eclipsed and staggered predictions continue at both low and high k . For all comparisons, in contrast to Fc, there is a clear preference for the staggered form of DmFc. This is in qualitative agreement with the results of our preliminary study⁶ and with the

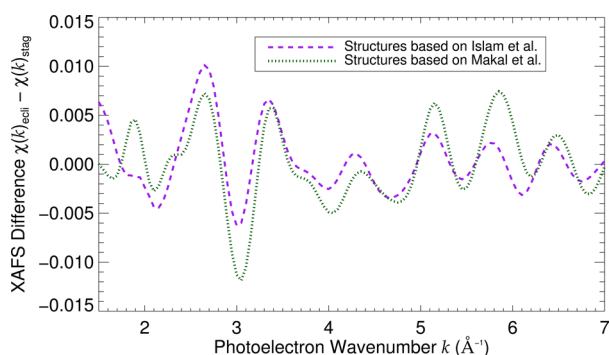


Figure 4. Difference between the XAFS spectra for eclipsed and staggered conformers based on the structures of Makal et al.¹⁹ and Islam et al.⁶ The XANES region shows the greatest sensitivity, as expected, for both structures; however, the prevalence of highly degenerate multiple scattering paths from the methyl carbons contributes some sensitivity in the higher energy regime.

prediction from steric hindrance, albeit with much greater significance.

For the structure reported by Islam et al., the difference in χ_r^2 between the conformers is close to 10% across all energies studied. The structures based upon Makal et al., however, show even greater significance due to markedly better agreement with experiment. In the full range, the χ_r^2 is halved. They also show a greater difference between conformers—as high as 20% in the low-energy regime.

These fits demonstrate that for a robust representation of DmFc, strong evidence exists for a staggered conformation across all of the energies considered in our analysis. The added conformational sensitivity at high k in DmFc is largely due to the abundance of highly degenerate carbon scattering paths, which contribute strongly to the XAFS spectrum. We are therefore able to conclude convincingly that the ground-state DmFc observed in the experiment exists in a staggered geometry, and to use this to confirm the significance of the conclusions for Fc being in the eclipsed conformation.

These results provide compelling evidence for the dominant ground-state conformations of Fc and DmFc, and the conclusions must be evaluated in terms of their relative level of significance and rigor. The χ_r^2 values in this work seem larger compared with the previous investigation using the FEFF and IFEFFIT-like multiple-scattering packages; however, this is a product of the higher effective uncertainties in $\chi(k)$ at high energies. Consequently, higher- k XAFS analysis provides less physical insight, particularly with regards to stereochemistry. In the region of overlap between the studies, the IFEFFIT-like fits⁶ are marginally better due to a more sophisticated fitting of background absorption, but below 3.5 \AA^{-1} the FEFF structures become unphysical, producing χ_r^2 values of order tens of thousands compared to FDMX values of order 5–10. IFEFFIT-like also optimizes the first structural cumulant, α , which corresponds to an expansion parameter adjusting the bond lengths separately for the eclipsed and staggered geometries. This can, in some cases, exaggerate the difference between conformations in the high-energy regime. The studies performed here with FDMX compare the conformations directly in the extended XANES region, where their difference signatures are strongest, meaning that differences seen in χ_r^2 values can be ascribed a much greater physical significance in this work where a full-potential modeling is used. Of course, some studies have interpreted crystallographic data to imply a

minimum angle intermediate between the ideal conformers, or potentially corresponding to a weighted combination. The statistical information quality is sufficient to ask and investigate this question in future work.

In view of the subtle distinction between the staggered and eclipsed isomers, these results represent a significant advance in the application of XAS methods for stereochemical analysis. They present new opportunities for the characterization of the solution-state metal complexes which underpin molecular and biomolecular catalysis. It has long been recognized that the detailed multiple-scattering behavior of the photoelectron, which is the key aspect of XAFS directly probing conformations of these compounds, is manifest most clearly in the extended XANES region. It is only now with the recent tools of FDMX that such spectra can be analyzed in a rigorous, self-consistent, and quantitative fashion.

■ ASSOCIATED CONTENT

§ Supporting Information

The Supporting Information is available free of charge on the ACS Publications website at DOI: [10.1021/acs.jpcllett.6b01382](https://doi.org/10.1021/acs.jpcllett.6b01382).

Methods describing in more technical detail the nature of the theoretical computation and fitting; results describing in more detail the quality of the data and the parameters investigated; detailed plots of k^2 -weighted spectra (PDF)

■ AUTHOR INFORMATION

Corresponding Author

*E-mail: chantler@unimelb.edu.au.

Notes

The authors declare no competing financial interest.

■ ACKNOWLEDGMENTS

We acknowledge the ARC for funding this work. We thank the staff of the Australian National Beamline Facility (ANBF), Tsukuba, Japan, where the experiment was performed. As the ANBF is now closed, we dedicate this work to the Australian and Japanese scientists who made the beamline and collaboration such a success.

■ REFERENCES

- (1) Seeman, J. I.; Cantrill, S. Wrong but seminal. *Nat. Chem.* **2016**, *8*, 193–200.
- (2) Werner, H. At least 60 years of ferrocene: the discovery and rediscovery of the sandwich complexes. *Angew. Chem., Int. Ed.* **2012**, *51*, 6052–6058.
- (3) Conroy, D.; Moisala, A.; Cardoso, S.; Windle, A.; Davidson, J. Carbon nanotube reactor: Ferrocene decomposition, iron particle growth, nanotube aggregation and scale-up. *Chem. Eng. Sci.* **2010**, *65*, 2965–2977.
- (4) Biot, C.; Nosten, F.; Fraisse, L.; Ter-Minassian, D.; Khalife, J.; Dive, D. The antimalarial ferroquine: from bench to clinic. *Parasite (Paris, France)* **2011**, *18*, 207–214.
- (5) Gasser, G.; Metzler-Nolte, N. The potential of organometallic complexes in medicinal chemistry. *Curr. Opin. Chem. Biol.* **2012**, *16*, 84–91.
- (6) Islam, M. T.; Best, S. P.; Bourke, J. D.; Tantau, L. J.; Tran, C. Q.; Wang, F.; Chantler, C. T. Accurate X-ray absorption spectra of dilute systems: Absolute measurements and structural analysis of ferrocene and decamethyl ferrocene. *J. Phys. Chem. C* **2016**, *120*, 9399–9418.
- (7) Mohammadi, N.; Ganesan, A.; Chantler, C. T.; Wang, F. Differentiation of ferrocene D_{5d} and D_{5h} conformers using IR spectroscopy. *J. Organomet. Chem.* **2012**, *713*, 51–59.

(8) Glover, J. L.; Chantler, C. T.; Soldatov, A. V.; Smolentsev, G.; Feiters, M. C. Theoretical XANES Study of the Activated Nickel (t-Amylisocyanide) Molecule. *AIP Conf. Proc.* **2006**, *882*, 625–627.

(9) Bourke, J. D.; Chantler, C. T.; Joly, Y. FDMX: extended X-ray absorption fine structure calculations using the finite difference method. *J. Synchrotron Radiat.* **2016**, *23*, 551–559.

(10) Joly, Y. X-ray absorption near-edge structure calculations beyond the muffin-tin approximation. *Phys. Rev. B: Condens. Matter Mater. Phys.* **2001**, *63*, 125120.

(11) Chantler, C. T.; Bourke, J. D. Full-potential theoretical investigations of electron inelastic mean free paths and extended x-ray absorption fine structure in molybdenum. *J. Phys.: Condens. Matter* **2014**, *26*, 145401.

(12) Tantau, L.; Chantler, C.; Bourke, J.; Islam, M.; Payne, A.; Rae, N.; Tran, C. Structure determination from XAFS using high-accuracy measurements of x-ray mass attenuation coefficients of silver, 11 keV–28 keV, and development of an all-energies approach to local dynamical analysis of bond length, revealing variation of effective thermal contributions across the XAFS spectrum. *J. Phys.: Condens. Matter* **2015**, *27*, 266301.

(13) Seiler, P.; Dunitz, J. Low-temperature crystallization of orthorhombic ferrocene: structure analysis at 98 K. *Acta Crystallogr., Sect. B: Struct. Crystallogr. Cryst. Chem.* **1982**, *38*, 1741–1745.

(14) Chantler, C. T.; Islam, M. T.; Best, S. P.; Tantau, L. J.; Tran, C. Q.; Cheah, M. H.; Payne, A. T. High accuracy X-ray Absorption Spectra from mM solutions of nickel(II) complexes with multiple solutions using transmission XAS. *J. Synchrotron Radiat.* **2015**, *22*, 1008–1021.

(15) Cramer, S. P.; Eccles, T. K.; Kutzler, F.; Hodgson, K. O.; Doniach, S. Applications of x-ray photoabsorption spectroscopy to the determination of local structure in organometallic compounds. *J. Am. Chem. Soc.* **1976**, *98*, 8059–8069.

(16) Ruiz-Lopez, M. F.; Loos, M.; Goulon, J.; Benfatto, M.; Natoli, C. R. Reinvestigation of the EXAFS and XANES spectra of ferrocene and nickelocene in the framework of the multiple scattering theory. *Chem. Phys.* **1988**, *121*, 419–437.

(17) Bourke, J. D.; Chantler, C. T. Measurements of electron inelastic mean free paths in materials. *Phys. Rev. Lett.* **2010**, *104*, 206601–206604.

(18) Freyberg, D. P.; Robbins, J. L.; Raymond, K. N.; Smart, J. C. Crystal and molecular structures of decamethyl-manganocene and decamethyl-ferrocene. Static Jahn-Teller distortion in a metallocene. *J. Am. Chem. Soc.* **1979**, *101*, 892–897.

(19) Makal, A. M.; Plazuk, D.; Zakrzewski, J.; Misterkiewicz, B.; Wozniak, K. Experimental charge density analysis of symmetrically substituted ferrocene derivatives. *Inorg. Chem.* **2010**, *49*, 4046–4059.